REPORT DOCUMENTATION PAGE

Form Approved OMB NO. 0704-0188

1. REPORT DATE (DD-MM-YYYY)	2. REPORT TYPE	3. DATES COVERED (From - To)
	New Reprint	-

4. TITLE AND SUBTITLE
Assessment of systematic measurement errors for acoustic travel-time tomography of the atmosphere

5a. CONTRACT NUMBER
W911NF-10-1-0415

5b. GRANT NUMBER

5c. PROGRAM ELEMENT NUMBER
611102

6. AUTHORS
Sergey N. Vecherin, Vladimir E. Ostashev, D. Keith Wilson

5d. PROJECT NUMBER

5e. TASK NUMBER

5f. WORK UNIT NUMBER

7. PERFORMING ORGANIZATION NAMES AND ADDRESSES
University of Colorado - Boulder
3100 Marine Street Room 479
572 UCB
Boulder, CO 80303 -1058

8. PERFORMING ORGANIZATION REPORT NUMBER

9. SPONSORING/MONITORING AGENCY NAME(S) AND ADDRESS(ES)
U.S. Army Research Office
P.O. Box 12211
Research Triangle Park, NC 27709-2211

10. SPONSOR/MONITOR'S ACRONYM(S)
ARO

11. SPONSOR/MONITOR'S REPORT NUMBER(S)
57813-EV.8

12. DISTRIBUTION AVAILIBILITY STATEMENT
Approved for public release; distribution is unlimited.

13. SUPPLEMENTARY NOTES
The views, opinions and/or findings contained in this report are those of the author(s) and should not contrued as an official Department of the Army position, policy or decision, unless so designated by other documentation.

14. ABSTRACT
see attached

15. SUBJECT TERMS
systematic errors, acoustic tomographyy, atmospheric turbulence

16. SECURITY CLASSIFICATION OF:			17. LIMITATION OF ABSTRACT	15. NUMBER OF PAGES	19a. NAME OF RESPONSIBLE PERSON
a. REPORT	b. ABSTRACT	c. THIS PAGE			Vladimir Ostashev
UU	UU	UU	UU		19b. TELEPHONE NUMBER: 303-497-3712

Report Title

Assessment of systematic measurement errors for acoustic travel-time tomography of the atmosphere

ABSTRACT

see attached

REPORT DOCUMENTATION PAGE (SF298)
(Continuation Sheet)

Continuation for Block 13

ARO Report Number 57813.8-EV
Assessment of systematic measurement errors ...

Block 13: Supplementary Note

Approved for public release; distribution is unlimited.

Assessment of systematic measurement errors for acoustic travel-time tomography of the atmosphere

Sergey N. Vecherin[a)]
U.S. Army Cold Regions Research and Engineering Laboratory, 72 Lyme Road, Hanover, New Hampshire 03755

Vladimir E. Ostashev
Cooperative Institute for Research in Environmental Sciences, University of Colorado at Boulder, 325 Broadway, Boulder, Colorado 80305

D. Keith Wilson
U.S. Army Cold Regions Research and Engineering Laboratory, 72 Lyme Road, Hanover, New Hampshire 03755

(Received 29 October 2012; revised 30 May 2013; accepted 28 June 2013)

Two algorithms are described for assessing systematic errors in acoustic travel-time tomography of the atmosphere, the goal of which is to reconstruct the temperature and wind velocity fields given the transducers' locations and the measured travel times of sound propagating between each speaker-microphone pair. The first algorithm aims at assessing the errors simultaneously with the mean field reconstruction. The second algorithm uses the results of the first algorithm to identify the ray paths corrupted by the systematic errors and then estimates these errors more accurately. Numerical simulations show that the first algorithm can improve the reconstruction when relatively small systematic errors are present in all paths. The second algorithm significantly improves the reconstruction when systematic errors are present in a few, but not all, ray paths. The developed algorithms were applied to experimental data obtained at the Boulder Atmospheric Observatory.
 [http://dx.doi.org/10.1121/1.4816411]

PACS number(s): 43.28.We, 43.28.Vd, 43.28.Gq [PBB] Pages: 1802–1813

I. INTRODUCTION

The goal of acoustic travel-time tomography is to reconstruct physical properties of the medium given the coordinates of speakers and microphones and the travel times of sound impulses propagating through the medium. In tomography of the atmosphere, the medium properties of interest are the temperature and wind velocity fields within an area (two-dimensional problem)[1–6] or volume (three-dimensional problem).[7,8] Mathematically, this problem belongs to the class of ill-posed problems; namely, the solution may not be unique for a given set of data. For example, some wind velocity fields with non-zero divergence (i.e., with volume sources or sinks) may not affect travel times along the sound propagation paths.[9–12] Moreover, there may exist temperature and wind velocity fluctuations that are too small to be resolved, given the spatial sampling of the available paths. Such fields are undetectable by travel-time tomography without supplementary data and are not considered in this paper.

The need to properly estimate and eliminate systematic errors is encountered in many disciplines. Estimation algorithms can be grouped into two categories: (1) algorithms for the estimation and prediction of the systematic errors owing to incompleteness of the numerical model of a physical phenomena being modeled[13–16] and (2) statistical algorithms for the systematic errors in the measured data.[17,18] The focus of this paper is on the second category, when reconstruction of the atmospheric fields is done using travel-time tomography.

In acoustic tomography experiments, the transducers' coordinates and the travel times of sound propagation between speakers and microphones should be measured accurately. The travel-time measurements include assessment of the time delays in electronic circuits and mechanical hardware (e.g., drivers and microphones) of a tomography array. References 4 and 5 already discussed the effect of random errors in the travel times on the tomographic reconstruction. The present paper considers systematic errors in the travel times that may be significantly larger than random errors and, thus, can significantly affect the quality of the reconstruction of temperature and wind velocity fields.

Several factors can contribute to the systematic errors in the travel-time measurements of acoustic tomography of the atmosphere. First, the systematic errors are caused by the errors in measurements of the time delays of signal propagation in hardware and electronic circuits of the tomography array and errors in synchronization of the transmitted and recorded signals. For example, if synchronization is done using the computer operating system, the corresponding systematic error can be of order 1 ms. Second, the errors in transducers coordinates can be as large as 30 cm. These errors are equivalent to the systematic errors in the travel times of 0.9 ms. Third, loudspeakers which are used in acoustic tomography are extended sources. To simplify a tomography experiment with many speakers and microphones (or if a tomography array needs to be assembled quickly),

a)Author to whom correspondence should be addressed. Electronic mail: sergey.n.vecherin@usace.army.mil

 0001-4966/2013/134(3)/1802/12/$30.00

this fact can be ignored in the mathematical formulation and loudspeakers can be considered as point sources. This approximation can result in the systematic errors of the coordinates of the effective point sources of order 1 m, which is equivalent to 3 ms. Finally, there might be other sources of systematic errors which are difficult to identify but which can be as large as those mentioned above.

The systematic errors might slowly change in time because of changing conditions in electronic circuits, mechanical hardware, and the positions of transducers. The importance of error analysis in tomography problems is well understood and the assessments of their influence on the reconstructions are available.[2,13,19–21] The current paper is focused on the techniques to mitigate these errors, which despite all efforts for their elimination are still present in the data. The paper describes two algorithms for an explicit assessment of the systematic errors from the corrupted travel-time measurements and discusses the effect of these systematic errors on the quality of the reconstruction. First, the algorithms are tested on numerically simulated temperature and wind velocity fields using large eddy simulation (LES).[22] Then, by applying the algorithms to experimental data obtained at the Boulder Atmospheric Observatory (BAO),[23] the paper shows how the algorithms can improve tomographic reconstructions.

II. PROBLEM STATEMENT

The basic equation for the reconstruction of temperature and wind velocity fields can be found, for example, in Refs. 4 and 7. In particular, the two-dimensional, linearized problem is described by the following equation:

$$t_i^{tr}(t) = \frac{L_i}{c_0(t)}\left[1 - \frac{u_0(t)\cos\varphi_i + v_0(t)\sin\varphi_i}{c_0(t)}\right] - F(t) + \varepsilon_i(t), \quad (1)$$

where t_i^{tr} is the travel time along the ith sound propagation path; $i = 1, 2, \ldots, I$; t is the time at which the measurement was performed; L_i is the length of the ith path; c_0 is the spatial mean sound speed in the motionless medium; u_0 and v_0 are the x and y Cartesian components of the spatial mean two-dimensional wind velocity; φ_i is the angle between the positive direction of the x axis and the direction of the ith path; and ε_i represents the random errors in measurements of the travel times. In Eq. (1), F accounts for travel-time contributions caused by fluctuations of the temperature $T(\mathbf{r}, t)$ and wind velocity $[u(\mathbf{r}, t), v(\mathbf{r}, t)]$ in the tomographic area relative to T_0 and c_0, respectively,

$$F(t) = \frac{1}{c_0^2(t)}\int_{L_i} \mathrm{dl}\left[\frac{c_0(t)}{2T_0(t)}T(\mathbf{r},\mathrm{t}) + u(\mathbf{r},t)\cos\varphi_i + v(\mathbf{r},t)\sin\varphi_i\right], \quad (2)$$

where $\mathbf{r} = (x, y)$ is the two-dimensional space vector, the integration is implemented along the ray path, and T_0 is the spatial mean temperature related to c_0 by a formula $c_0^2 = \gamma R_a T_0$ with $\gamma \approx 1.40$ being the ratio of the specific heats and $R_a \approx 287.058$ J/(kg K) being the specific gas constant for dry air. The formulation given by Eqs. (1) and (2) assumes straight-line sound propagation, which is valid if the vertical gradients of temperature and wind magnitude are small, so that the rays belong to a single plane, and the total wind fields and temperature fluctuations much smaller than the mean sound speed and mean temperature, respectively: $|u_0 + u|/c_0 \ll 1$, $|v_0 + v|/c_0 \ll 1$, and $|T|/T_0 \ll 1$. Keeping only the first-order powers of these small ratios and using the results in Sec. 3.3.1 of Ref. 24, it can be shown that $\mathbf{n}\cdot\mathbf{s} = 1$. Therefore, in this approximation, the unit vectors $\mathbf{n}$ (normal to a wave front) and $\mathbf{s}$ (direction of impulse propagation) coincide. As shown in Ref. 1, the linear approximation in acoustic tomography of the atmosphere introduces negligible errors for relatively short sound propagation paths on the order of 200 m. The temperature in Eq. (2) represents the acoustic virtual temperature, $T_{av} = T_0 + T$. A thermodynamic temperature T_{th} can be recalculated from the acoustic virtual temperature using the following relationship [Eq. (6.23) in Ref. 24]: $T_{av} \cong T_{th}(1 + 0.511q)$, where q is the specific humidity of air. As discussed in Refs. 9–12, for a unique reconstruction of $u(\mathbf{r}, t)$, and $v(\mathbf{r}, t)$, we shall assume that their sources and sinks are negligible at each time t, that is $\partial u(\mathbf{r},t)/\partial x + \partial v(\mathbf{r},t)/\partial y \approx 0$. The actual assumption employed in LES is $\partial u(\mathbf{r},t)/\partial x + \partial v(\mathbf{r},t)/\partial y + \partial w(\mathbf{r},t)/\partial z = 0$, as valid for an incompressible, three-dimensional fluid. The analysis of the LES fields used in this paper corroborated validity of the small two-dimensional divergence assumption.

The reconstruction of the temperature and wind velocity fields can be implemented in two stages, as proposed in Ref. 4. First, the mean values of the sound speed and wind velocity components are reconstructed via the least-squares fit using Eq. (1) with the $F(t)$ term omitted. This reconstruction will be called "Algorithm 1" in this paper. Estimation of the variance of the reconstruction errors due to measurement errors ε_i is implemented by a standard error estimation technique[25] that assumes independence of the measurement errors, both in repeated measurements for the same sound path and between any two paths. Then, the $F(t)$ term is calculated using Eq. (1), which enters as the input data in the left-hand side of Eq. (2) for the reconstruction of the temperature and wind velocity fluctuations using the time-dependent stochastic inversion (TDSI) algorithm.[4–7] The advantage of TDSI, compared to other inverse techniques, is that it uses data measured multiple times to reconstruct the fluctuations at one particular time (effectively increasing the amount of data), incorporating known spatial-temporal correlations of the fluctuations into the reconstruction.

The problem with Algorithm 1 is that the travel times t_i^{tr} can be corrupted by the systematic errors d_i which are constant or slowly changing in time and might be different for each path i. There are two principal distinctions between systematic and random errors. First, systematic errors are constant (or vary slowly) from one measurement to another while random errors are independent and have zero mathematical expectation. Second, their magnitudes might be larger than that of ε_i. As demonstrated in Sec. IV, large

systematic errors in the travel times make the reconstruction of temperature and wind velocity impossible. The goal of this paper is to investigate whether these systematic errors in the travel times can be explicitly estimated from the measurements and, consequently, eliminated from the data.

III. METHOD

Our procedure for estimating systematic errors assumes that these errors are constant in a series of repeated measurements of the travel times during some time interval Δt. It is assumed that systematic errors with a weak trend can also be treated this way, if they are nearly constant during the interval of data measurements Δt, which was equal to 10 s in the outdoor and numerical experiments. Let d_i be a systematic error in the ith ray. Then, Eq. (1) can be recast as

$$t_i^{tr}(t) = \frac{L_i}{c_0}\left(1 - \frac{u_0 \cos\varphi_i + v_0 \sin\varphi_i}{c_0}\right) - F(t) + \varepsilon_i(t) + d_i, \quad t \in \Delta t. \tag{3}$$

Unlike Eq. (1), the mean values c_0, u_0, and v_0, as well as the errors d_i, are considered as constants during the time interval Δt for which Eq. (3) is applied. This does not introduce any additional errors or inconsistencies in the reconstruction algorithm outlined above. The only difference is that the mean values c_0, u_0, and v_0 are now not instantaneous spatial mean values but the spatial-temporal mean values over the tomographic area defined by the tomographic setup and over the time interval Δt. This, of course, changes the estimation of $F(t)$ and, consequently, the reconstructed temperature and wind velocity fluctuations. As before, the reconstruction of these mean values is implemented by neglecting the fluctuation term $F(t)$ in Eq. (3). However, unlike the original Algorithm 1, the mean values are estimated *simultaneously* with the unknown systematic errors d_i, using the least-squares fit. Such an idea was exploited in underwater acoustic tomography in a variety of reconstruction techniques.[26–28] This reconstruction will be referred to as "Algorithm 2." Note that one needs to use data from several measurements to make the problem over determined. Indeed, a set of travel-time measurements implemented at some time $t_1 \in \Delta t$ has I data and $I + 3$ unknowns (c_0, u_0, v_0, and all d_i's). Using data from another consecutive measurement at $t_2 \in \Delta t$, one has $2I$ data and still $I + 3$ unknowns. Thus, for $I > 3$, one should use at least two data sets acquired at two different times. To

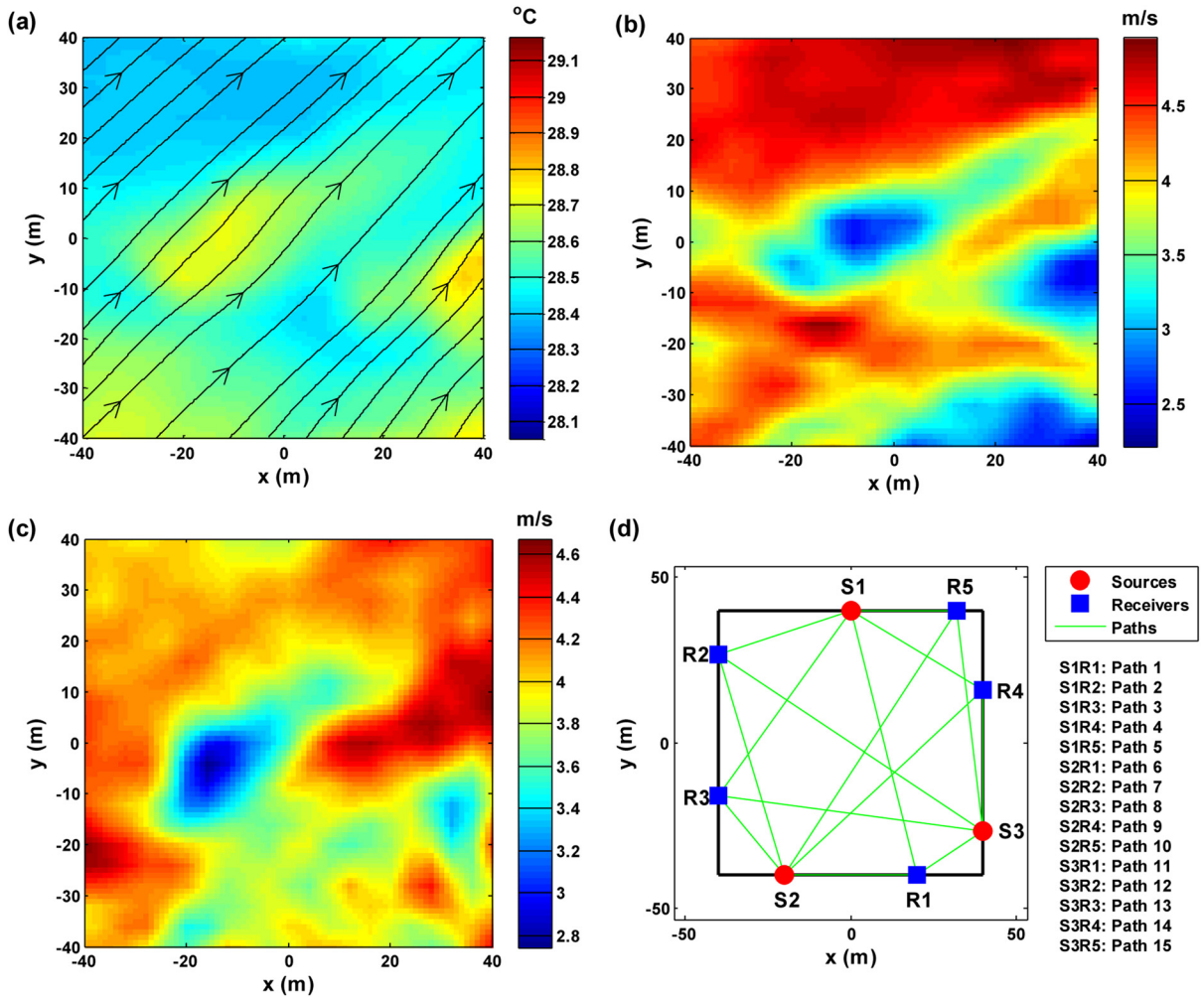

FIG. 1. (Color online) LES fields used in the numerical study. (a) Temperature field. Black streamlines with arrows indicate wind direction. (b) First horizontal component of the wind velocity vector, $u_0 + u$. (c) Second horizontal component of the wind velocity vector, $v_0 + v$. (d) Principal schema of the tomography sensor array.

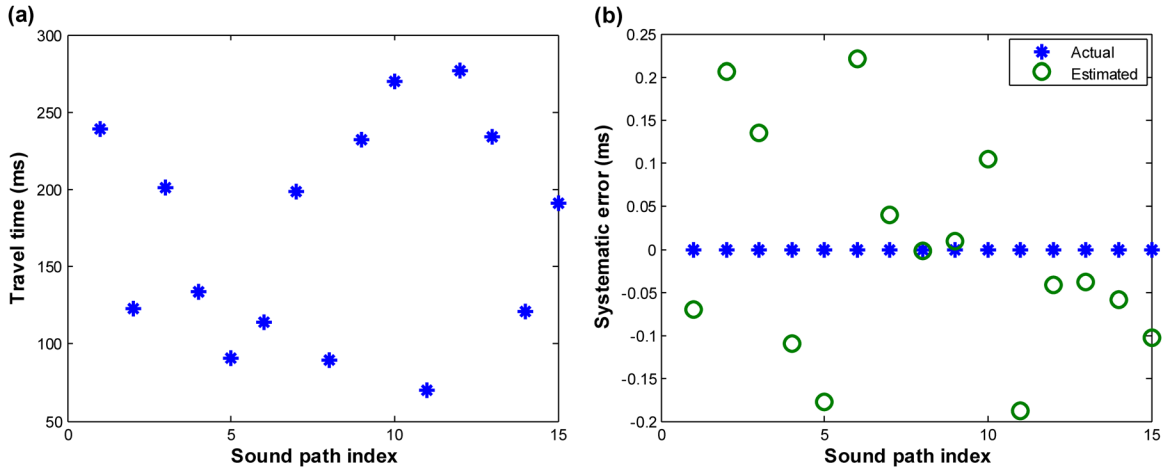

FIG. 2. (Color online) (a) Travel times for the 15 paths shown in Fig. 1(d). (b) Actual (asterisks) and estimated (circles) systematic errors in the travel times. Note that the actual systematic errors are zeros for this case.

increase the robustness and reduce the errors of the estimation, more data can be used. The reconstruction of the fluctuations is then performed by the TDSI algorithm, as before. In the next section, the proposed method is studied in numerical experiments with simulated temperature and wind velocity fields.

IV. NUMERICAL STUDY

For this study, atmospheric temperature and wind velocity fields were created using LES[22] that represents realistic atmospheric fields. In LES, the Navier–Stokes equations are solved numerically for relatively large spatial scales (in our case, larger than 4 m), while the fields at smaller scales are parameterized depending on the regime of the atmosphere and ground conditions. In the present study, a two-dimensional slice (at a height of 13.75 m) of the fields corresponding to a typical unstable atmosphere over a homogeneous ground was used. The frozen turbulence hypothesis[29,30] was used to create temporal evolution of turbulence from the two-dimensional slice of the LES fields. According to this hypothesis, turbulence translates, without distortion, at a constant advection velocity. In our numerical simulations, the advection velocity was set to have Cartesian components of (4, 4) m/s. These time-dependent fields allowed us to calculate travel times t_i^{tr} for different times t simulating physical measurements. A realization of the temperature and wind velocity fields to be reconstructed and the tomographic setup are shown in Fig. 1. Black streamlines with arrows in Fig. 1(a) indicate the direction of wind. Figures 1(b) and 1(c) depict the components of the wind velocity, $u_0 + u$ and $v_0 + v$, respectively. Figure 1(d) shows the tomographic setup consisting of five microphones and three speakers. This figure is a view from above on the BAO acoustic tomography array. For a single scan, the setup provides 15 travel times corresponding to 15 rays. The travel times t_i^{tr} corresponding to the fields in Fig. 1 are shown in Fig. 2(a) versus the index i of a particular path. In the numerical simulations, the contributions to the travel times due to fluctuations [i.e., the term F in Eqs. (1)–(3)] were on the order of ± 4 ms. To be able to reconstruct the fluctuations, we need the accuracy of their measurements to be less than 10%. That is, a threshold of 0.4 ms was imposed as the acceptable error magnitude in travel times. Since the experimental setup at BAO was supposed to provide this accuracy, this value is also a threshold for deciding whether systematic errors are present in the data. The following cases are considered to investigate whether large but constant systematic errors can be effectively estimated and eliminated from the data.

A. Case 1

There are no systematic errors in the data. This case illustrates the situation when the data processing algorithm assumes the presence of the systematic errors, the least-squares fit is based on Eq. (3), but there are no systematic errors in reality. As shown in Fig. 2(b), the least-squares fit (Algorithm 2) yields artifact systematic errors (circles) ranging from -0.20 ms to 0.23 ms. For this estimate, travel times from five consecutive scans were used, providing 75 data points. As one can see in Table I, despite spurious reconstructed systematic errors, the reconstruction of the mean fields is accurate, as good as by the original Algorithm 1 designed for no systematic error reconstruction. Both algorithms yield close values and comparable estimated errors of the reconstruction.

B. Case 2

There is a systematic error in a single ray. For this case, a constant systematic error of 10 ms was added to the travel time of the sound impulse propagating along the third path, $i = 3$, which introduces a 5% error in the travel time. Note

TABLE I. Mean field reconstructions without systematic errors in the input data. "Algorithm 1" and "Algorithm 2" refer to the original algorithm without systematic errors and the proposed one, assuming systematic errors in all paths, respectively.

Mean fields	T (°C)	u (m/s)	v (m/s)
Actual	28.53	4.00	4.00
Algorithm 1	28.60 ± 0.09	4.03 ± 0.07	4.05 ± 0.07
Algorithm 2	28.50 ± 0.05	4.03 ± 0.04	4.10 ± 0.04

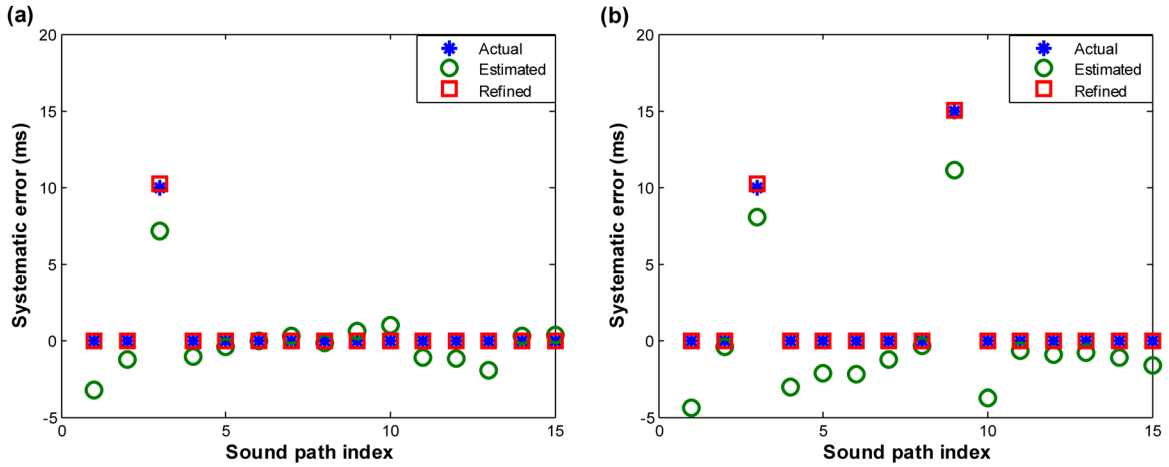

FIG. 3. (Color online) Actual (asterisks) and reconstructed systematic errors. Circles depict the Algorithm 2 estimate, assuming that systematic errors are present in all rays. Squares depict the estimation by Algorithm 3 when the path indices with systematic errors are determined from Algorithm 2. (a) One systematic error in path 3. (b) Two systematic errors in paths 3 and 9.

that 10 ms is of order of the combined systematic errors mentioned in Sec. I. Such a systematic error is prohibitively large for reconstruction of weak fluctuations. Without proper detection and elimination of such errors, the reconstruction will be severely distorted, as demonstrated below. In the outdoor experiments, Sec. V, the estimated systematic errors are on the order of 1 ms. Figure 3(a) depicts the actual systematic errors (asterisks) and the estimated systematic errors obtained with Algorithm 2 (circles), assuming that the errors exist for each ray. As one can see from Fig. 3(a), this algorithm does not provide a reliable estimate. Namely, the systematic error in a single ray causes spurious reconstructed systematic errors in all rays. Although the third (true) error is the largest, 7.2 ms, this is not a good estimation of the actual 10 ms error; their discrepancy is significantly larger than the imposed threshold of 0.4 ms. Additionally, the other errors are not of negligible magnitudes, ranging from −3.2 ms to 1.0 ms. Moreover, the mean field reconstructions by both algorithms become inaccurate; see "Algorithm 1" and "Algorithm 2" in Table II. The discrepancy between the actual and reconstructed mean fields is as large as 2.7 °C, 1.1 m/s, and 2.6 m/s for Algorithm 1 and 3.6 °C, 1.2 m/s, and 3.0 m/s for Algorithm 2. Note that the estimated reconstruction errors in the Algorithm 1 have increased by 1 order of magnitude in comparison with case 1 when the travel times were error free. Therefore, such large estimated errors can serve as indicators of the presence of systematic errors in the data.

TABLE II. Mean field reconstructions with a single systematic error. "Algorithm 1" and "Algorithm 2" refer to the algorithms, without systematic errors and assuming systematic errors in all paths, respectively. "Algorithm 3" refers to the refined estimation algorithm, assuming a systematic error in ray 3.

Mean fields	T (°C)	u (m/s)	v (m/s)
Actual	28.53	4.00	4.00
Algorithm 1	25.9 ± 0.9	5.1 ± 0.7	6.6 ± 0.7
Algorithm 2	24.95 ± 0.04	5.22 ± 0.04	7.03 ± 0.03
Algorithm 3	28.67 ± 0.09	4.01 ± 0.07	3.99 ± 0.08

To mitigate these problems, we propose a refined reconstruction, referred to as "Algorithm 3" hereafter. The idea is to use the results of the Algorithm 2 to determine which paths actually have the errors. Judging from Fig. 3(a), the largest estimated error occurs in the third path. Now, the least-squares estimation can be repeated analogously to Algorithm 2 with systematic errors, appearing in Eq. (3), but only a single systematic error is accounted for in the third path. The systematic errors of a reconstruction refined in this manner are shown in Fig. 3(a) by squares, and the reconstructed mean fields are shown in Table II. The refined reconstruction yields significantly better results. First, the estimated error in the third ray is 10.2 ms, which is very close to the actual value of 10 ms, with the discrepancy below the 0.4 ms threshold. Second, the mean field values are significantly better than in the two previous algorithms. The differences between the actual and reconstructed fields are small: 0.14 °C, 0.1 m/s, and 0.1 m/s. The estimated reconstruction errors have also decreased as compared to the original reconstruction by Algorithm 1. To validate the refined reconstruction approach (Algorithm 3), let us consider the following case.

C. Case 3

There are distinct systematic errors in two rays. The systematic errors of 10 and 15 ms were added to the third and ninth rays, respectively, which corresponds to the 5.0% and 6.5% relative errors in the third and ninth travel times. Figure 3(b) shows the actual (asterisks) and estimated (circles and

TABLE III. Mean field reconstructions with systematic errors in two paths. "Algorithm 1" and "Algorithm 2" refer to the algorithms without systematic errors and assuming systematic errors in all paths, respectively. "Algorithm 3" refers to the refined estimation algorithm assuming systematic errors in two paths.

Mean fields	T (°C)	u (m/s)	v (m/s)
Actual	28.53	4.00	4.00
Algorithm 1	24 ± 1	3 ± 1	5 ± 1
Algorithm 2	21.09 ± 0.04	0.96 ± 0.04	5.24 ± 0.03
Algorithm 3	28.66 ± 0.10	4.01 ± 0.07	3.99 ± 0.08

squares) systematic errors. As in Fig. 3(a), the circles stand for Algorithm 2 (the two largest estimates indicating the path indices with the systematic errors); and the squares depict the refined reconstruction of the systematic errors. Similarly to case 2, the refined reconstruction yields very accurate estimations: 10.2 ms for the actual 10 ms in the third travel time, and 15.0 ms for the actual 15 ms in the ninth travel time. The reconstruction of the mean fields by the three algorithms is summarized in Table III. With the systematic errors in two data points, Algorithm 1 and Algorithm 2 yield spurious

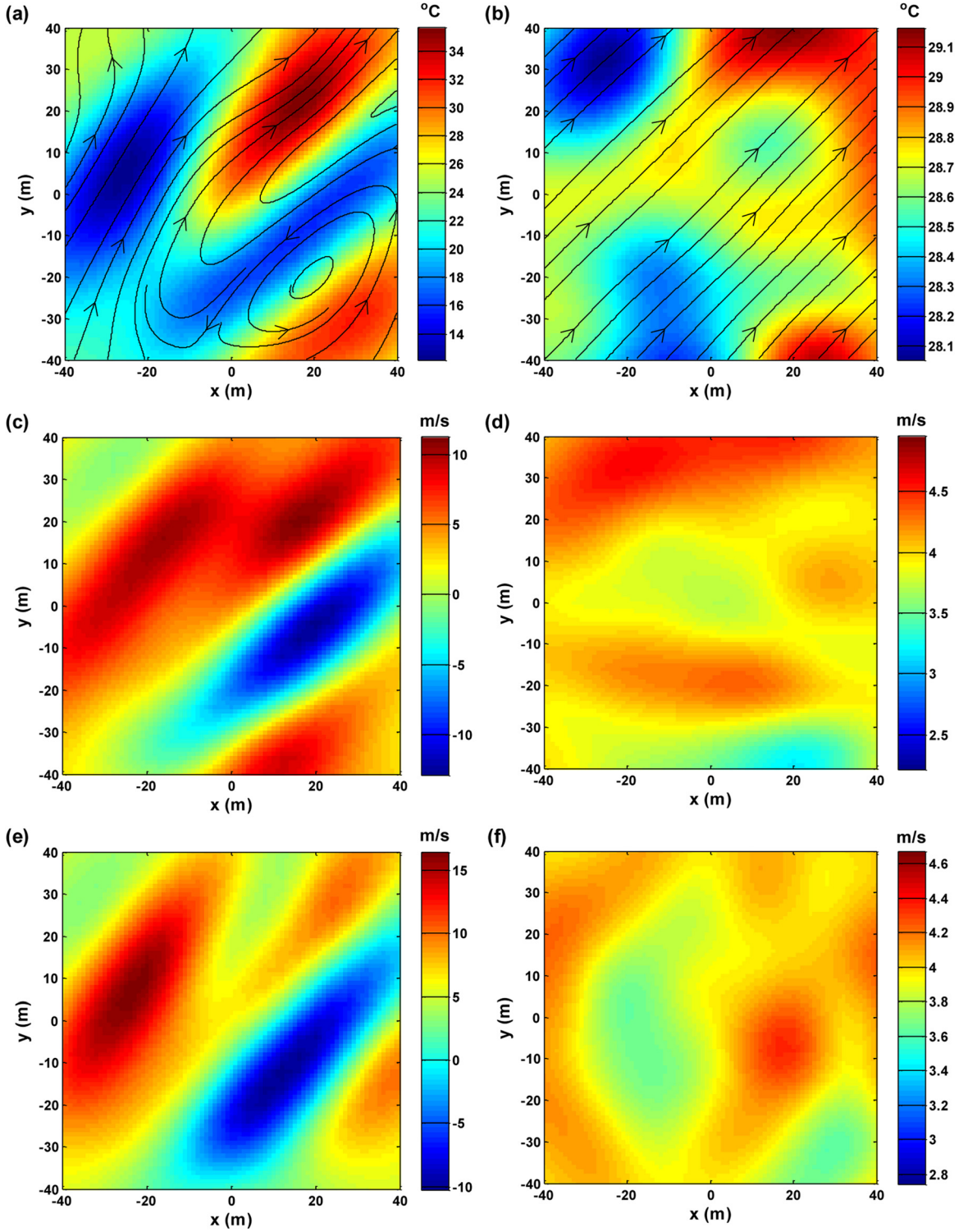

FIG. 4. (Color online) Reconstruction of the unstable LES fields in the presence of two constant systematic errors in paths 3 and 9. Note significant improvement in reconstructions (right column) when Algorithm 3 was used, correctly assuming systematic errors in paths 3 and 9. (a) Temperature field, no estimation of the systematic errors. (b) Temperature field, refined estimation of the systematic errors. (c) First horizontal component of the wind velocity vector, $u_0 + u$, no estimation of the systematic errors. (d) First horizontal component of the wind velocity vector, $u_0 + u$, refined estimation of the systematic errors. (e) Second horizontal component of the wind velocity vector, $v_0 + v$, no estimation of the systematic errors. (f) Second horizontal component of the wind velocity vector, $v_0 + v$, refined estimation of the systematic errors.

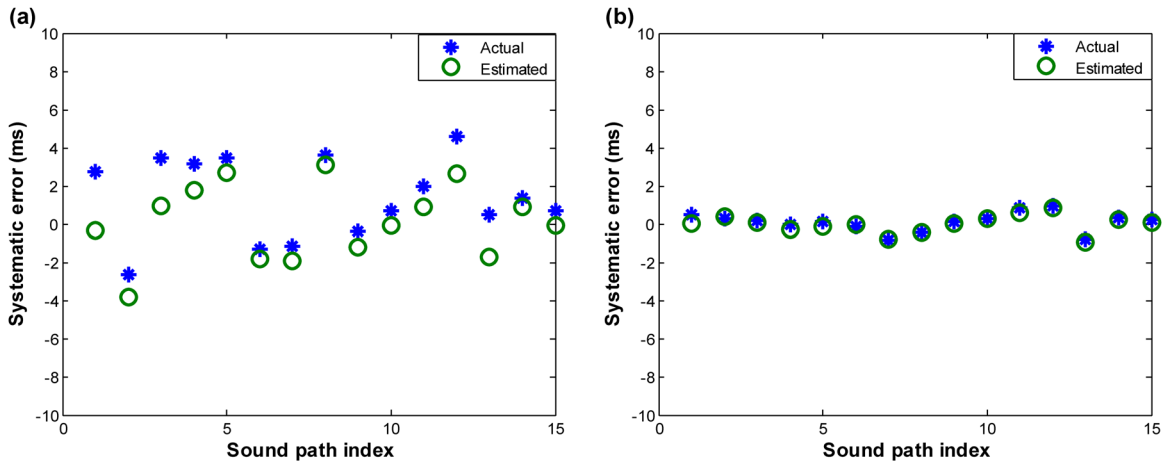

FIG. 5. (Color online) Actual (asterisks) and estimated by Algorithm 2 (circles) systematic errors present in all paths. (a) Large systematic errors in the interval [−5 5] ms. (b) Small systematic errors in the interval [−1 1] ms.

estimates. In contrast, Algorithm 3 yields not only the correct systematic errors but also accurate reconstructions of the mean fields (see Table III). Moreover, the reconstruction of the fluctuations and, thus, complete fields (Fig. 4) from these distorted data using the refined mean field reconstruction is also very good despite mismatched eddy distributions of the temperature field: Comparison of Fig. 1 and Fig. 4 reveals that Algorithm 3 yields reconstructions with average errors of order 0.5 °C and 0.5 m/s while Algorithm 1 yields spurious reconstructions with an error order of 7 °C and 7 m/s. Figures 4(a), 4(c), and 4(e) illustrate the spurious solution obtained by Algorithm 1 followed by TDSI for the reconstruction of the fluctuations from the two-path-error data. All fields are out of plausible ranges, and the shape of the fluctuations mismatches those of the actual fields shown in Fig. 1. In contrast, Algorithm 3 followed by TDSI, Figs. 4(b), 4(d), and 4(f), yields much better reconstructions, not only in the right range of values but also by capturing the actual shapes of some fluctuations; see, for example, the reconstruction of the u component.

D. Case 4

There are systematic errors in all rays. For this case, systematic errors randomly distributed in the range [−5, 5] ms were added to all travel times, introducing relative errors in the travel times ranging from 0.2% to 4%. Note that Algorithm 3, in this case, coincides with Algorithm 2. The actual and reconstructed systematic errors are shown in Fig. 5(a). None of the errors are reconstructed accurately enough resulting in a spurious reconstruction of the mean fields; see Table IV, rows "Alg. 1, large errors" and "Alg. 2, large errors." These results can be summarized as follows: If all input data to a reconstruction algorithm have large unknown systematic errors, as in the considered case 4, the correct reconstruction is impossible. However, if systematic errors are of small magnitude, this somewhat improves the situation. Figure 5(b) shows actual and reconstructed systematic errors when the actual ones are in the range [−1, 1] ms (relative errors in the travel times do not exceed 1.2%). In this case, the reconstruction of the mean fields becomes better, as one can see in Table IV, "Alg. 1, small errors" and "Alg. 2, small errors" rows. Note that Algorithm 2 yields slightly better estimations than the original Algorithm 1.

From the considered cases, we conclude that systematic errors in several, but not all, travel times can be successfully detected and eliminated by the refined reconstruction technique, Algorithm 3. Large estimated errors in the mean field reconstructions obtained by the original Algorithm 1 indicate possible presence of systematic errors in the data. If systematic errors are present in all data, their accurate estimation and mean field reconstruction are, generally, impossible. However, for small systematic errors, Algorithm 2 may provide better reconstruction of the mean fields than the original Algorithm 1.

Algorithms 1, 2, and 3 were also used in numerical analysis of the systematic errors for other LES fields corresponding to different snapshots of an unstable atmosphere, a very unstable atmosphere, and a neutral atmosphere. The results supported the tendencies described above. For example, Table V shows the mean field reconstructions for all cases studied above for very unstable LES, depicted in Figs. 6(a), 6(b), and 6(c). One can observe the same features as for the unstable LES: For errors in a single path and two paths, Algorithm 3 outperforms both Algorithm 1 and Algorithm 2. If large (±5 ms) errors are present in all paths, then all algorithms fail to reconstruct the fields. However, if the errors are small (±1 ms), the reconstruction converges to the actual fields, and Algorithm 2 slightly outperforms Algorithm 1.

These features are also clearly seen in Fig. 6. Figures 6(d), 6(e), and 6(f) depict failed reconstructions of temperature

TABLE IV. Mean field reconstructions with systematic errors in all input data. "Alg. 1" and "Alg. 2" refer to the algorithms without systematic errors and assuming systematic errors in all paths, respectively.

Mean fields	T (°C)	u (m/s)	v (m/s)
Actual	28.53	4.00	4.00
Alg. 1, large errors	22 ± 1	3.7 ± 0.9	5 ± 1
Alg. 2, large errors	23.56 ± 0.04	4.53 ± 0.04	5.74 ± 0.03
Alg. 1, small errors	27.8 ± 0.2	4.3 ± 0.2	4.8 ± 0.2
Alg. 2, small errors	28.02 ± 0.05	3.94 ± 0.04	4.35 ± 0.04

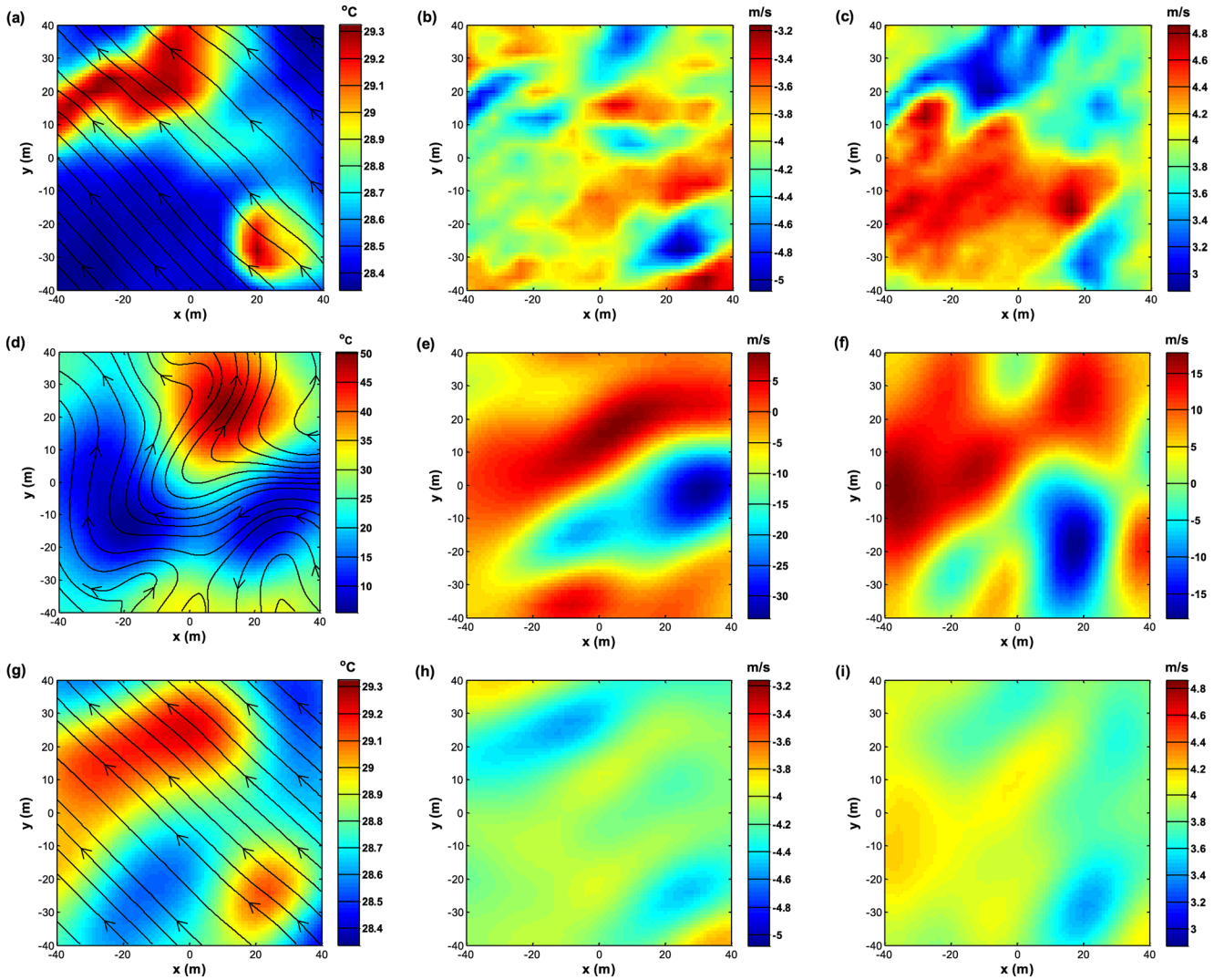

FIG. 6. (Color online) Reconstruction of a very unstable LES. (a) Actual temperature field. Black streamlines with arrows indicate wind direction. (b) Actual first horizontal component of the wind velocity vector, $u_0 + u$. (c) Actual second horizontal component of the wind velocity vector, $v_0 + v$. Reconstruction without estimation of the systematic errors (Algorithm 1) with two travel times present in paths 3 and 9: (d) Temperature. (e) $u_0 + u$. (f) $v_0 + v$. Reconstruction with the estimated systematic errors by Algorithm 3: (g) Temperature. (h) $u_0 + u$. (i) $v_0 + v$.

and wind velocity components, respectfully, with errors in two travel times. Note the unrealistic scale of the fluctuations: [5, 50] °C, [−33, 8] m/s, and [−17, 16] m/s. The wind direction, depicted by streamlines with arrows in Fig. 6(d), is also significantly distorted. In contrast, using travel times obtained with Algorithm 3, the reconstructions become relatively accurate, see Figs. 6(g), 6(h), and 6(i). The magnitudes of all fields are slightly underestimated, but the main features of the actual fields are captured correctly. For example, in Fig. 6(g), the locations and shapes of the two eddies are correctly estimated with respect to the actual temperature field shown in Fig. 6(a). The similarity of the wind velocity components is less obvious, but the locations of "fast" and "slow" eddies and their orientation are captured with the discrepancy in the wind velocity magnitude of approximately 0.3–0.4 m/s.

V. EXPERIMENTAL DATA

We now apply results from the previous section to experimental data obtained at the BAO. The experiment was conducted on 9 July 2008, 21:32 UTC at the BAO. Eight bend-over towers with three speakers and five microphones were located at a height of 9 m, at positions shown in

TABLE V. Mean field reconstructions of very unstable LES fields with Algorithm 1, Algorithm 2, and Algorithm 3.

Case	Algorithm	T (°C)	u (m/s)	v (m/s)
Actual		28.65	−4.00	4.00
Single error	Algorithm 1	26.1 ± 0.8	−2.9 ± 0.6	6.4 ± 0.7
	Algorithm 2	25.32 ± 0.06	−2.78 ± 0.05	6.87 ± 0.05
	Algorithm 3	28.80 ± 0.06	−4.10 ± 0.04	3.93 ± 0.05
Two errors	Algorithm 1	24 ± 1	−5 ± 1	5 ± 1
	Algorithm 2	21.5 ± 0.06	−6.9 ± 0.05	5.08 ± 0.05
	Algorithm 3	28.8 ± 0.06	−4.13 ± 0.04	3.91 ± 0.05
Large errors ±5 ms	Algorithm 1	26 ± 2	−2 ± 1	7 ± 1
	Algorithm 2	26.6 ± 0.06	−2.33 ± 0.05	5.50 ± 0.05
Small errors ±1 ms	Algorithm 1	27.0 ± 0.3	−4.4 ± 0.2	4.2 ± 0.2
	Algorithm 2	27.51 ± 0.06	−4.22 ± 0.05	3.90 ± 0.05

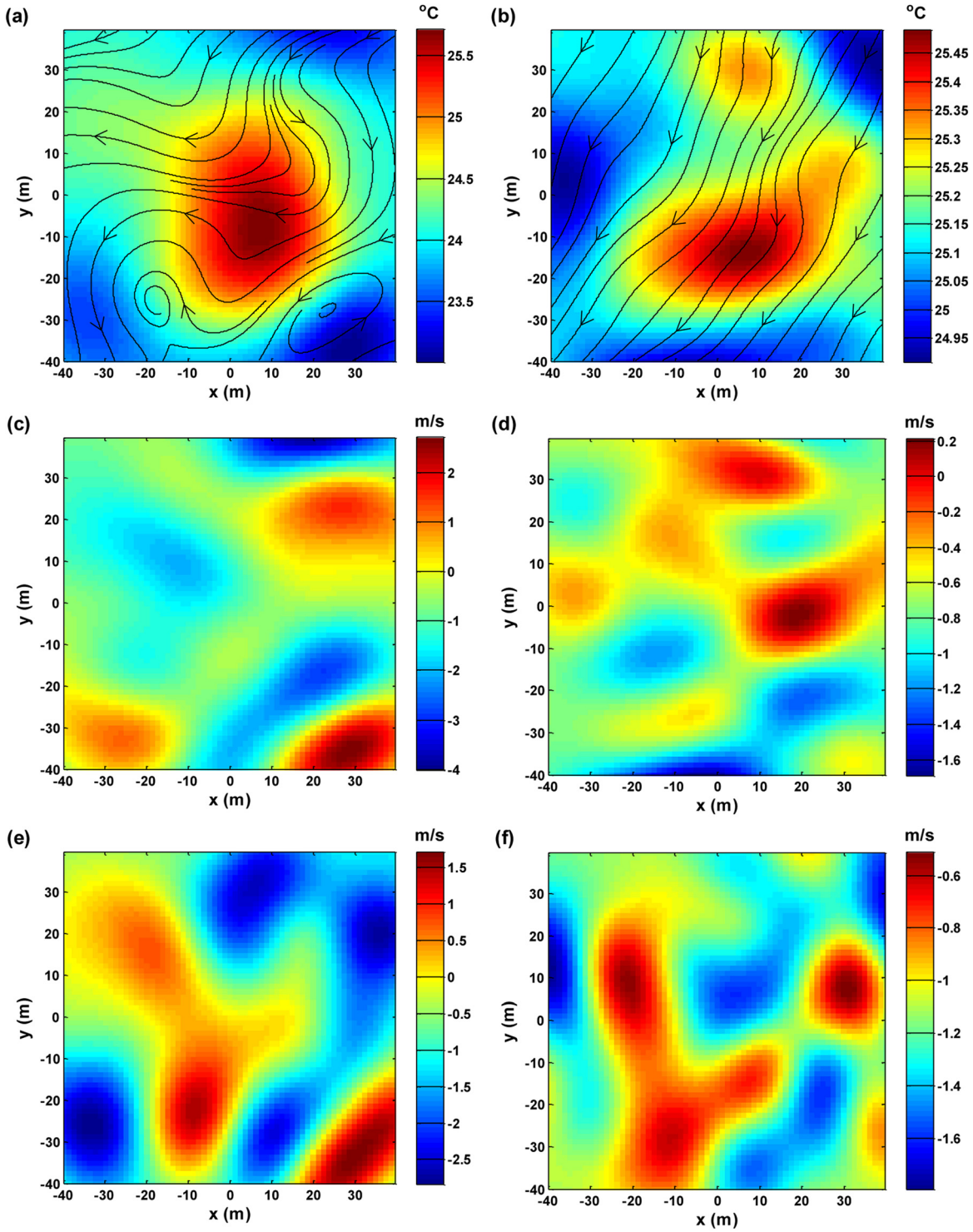

FIG. 7. (Color online) Reconstruction the fields in the BAO experiment on 9 July 2008, 21:32 UTC. Note significant improvement in reconstructions (right column) when Algorithm 3 was used. (a) Temperature field, no estimation of the systematic errors. (b) Temperature field, refined estimation of the systematic errors. (c) First horizontal component of the wind velocity vector, $u_0 + u$, no estimation of the systematic errors. (d) First horizontal component of the wind velocity vector, $u_0 + u$, refined estimation of the systematic errors. (e) Second horizontal component of the wind velocity vector, $v_0 + v$, no estimation of the systematic errors. (f) Second horizontal component of the wind velocity vector, $v_0 + v$, refined estimation of the systematic errors.

Fig. 1(d). The systematic errors in the travel times during this experiment might have been caused by errors in time delays estimates and transducers' coordinates that were not measured at the time of the experiment. (Such measurements are costly, are time consuming, and are done at the BAO tomography array only from time to time). Furthermore, after a previous experiment, the towers of the BAO array were bent over and then elevated again so that the measured transducer's coordinates might not exactly coincide with those during the experiment. Thus, the experiment on 9 July 2008

TABLE VI. Mean field reconstructions for experimental data. "Algorithm 1" and "Algorithm 3" refer to the algorithms without systematic errors and the refined reconstruction, respectively.

Mean fields	T (°C)	u (m/s)	v (m/s)
Algorithm 1	24.0 ± 0.3	−0.67 ± 0.3	−0.68 ± 0.3
Algorithm 3	25.14 ± 0.09	−0.71 ± 0.07	−1.11 ± 0.07

presents a good opportunity to study the reconstruction of temperature and wind velocity fields in the presence of possible systematic errors in the travel times.

Table VI shows the mean field reconstructions by Algorithm 1 and Algorithm 3. Figures 7(a), 7(c), and 7(e) depict the full reconstructed temperature and wind velocity component fields, respectively. As one can see, the reconstruction by the original algorithm looks unrealistic. First, the ranges of variations are [23.0, 25.6] °C for the temperature field and [−4.0, 2.5] m/s and [−2.60, 1.55] m/s for the wind velocity components, which seem implausibly large for the 80 m by 80 m tomography area. Second, the wind flow depicted by black lines in Fig. 7(a) is dramatically curled, which also appears unrealistic. This is reminiscent of Figs. 4(a), 4(c), and 4(e), indicating possible presence of the systematic errors in the measured travel times.

Figure 8 presents an analysis of systematic errors. The assessment of systematic errors assuming that they are present along all paths (Algorithm 2) are shown in Fig. 8(a). A more detailed analysis reveals that only six errors, corresponding to paths 5, 8, 10, 11, 12, and 15, have relatively large magnitudes, larger than 0.4 ms. Following the numerical case studies, the refined reconstruction by Algorithm 3 was implemented for more accurate systematic error assessments in these paths, whereas the systematic errors along other ray paths were set to zeros. The systematic errors for this reconstruction are shown in Fig. 8(b). The mean field reconstruction by Algorithm 3 is shown in Table VI, while the full fields are depicted in Figs. 7(b), 7(d), and 7(f). The ranges of variability of the reconstructed fields within the tomographic area have been significantly reduced. They are [24.9, 25.5] °C for the temperature field and [−1.65, 0.20] m/s and [−1.78, −0.55] m/s for the wind velocity components, which is more realistic. Also, the reconstructed air flow becomes more realistic; see Fig. 7(d).

Other acoustic tomography experiments at the BAO conducted at different meteo conditions (day, night, and distinct dates) were also processed. The results obtained were similar to those presented above, namely, the expected errors decreased using Algorithms 2 and 3, and the reconstructed fields had plausible ranges of variability. Figure 9 exemplifies a reconstruction of the fields on 11 August 2008, 21:31 UTC. Note that reconstructions implemented using Algorithm 1 have unrealistically wide ranges of variability: The temperature field varies from 21.1 °C to 26.2 °C [Fig. 9(a)], the first wind velocity component varies from −7 m/s to 0.4 m/s [Fig. 9(c)], and the second component lies in the range 0.8–9.5 m/s [Fig. 9(e)]. The reconstructions performed with Algorithm 3 are shown in Figs. 9(b), 9(d), and 9(f), respectively. Note plausible ranges that became of the same order of magnitude as in the LES numerical studies. These results corroborate those depicted in Fig. 7.

VI. SUMMARY AND CONCLUSIONS

Systematic errors in measured travel times can significantly distort tomographic reconstructions. This paper studied two algorithms aimed at assessing systematic errors present in the data. Simultaneous reconstruction of the fields and systematic errors, as considered previously in underwater acoustic tomography,[26–28] was performed. The numerical study suggests that it can be done successfully only if the systematic errors are present in a few, but not all, of the measured travel times. If all travel times are corrupted, a good reconstruction is generally impossible unless the systematic errors in travel times are small, on the order of 1% relative to travel times in the considered experiments. Based on these observations, we proposed the algorithm for refining reconstructions. The initial systematic error estimates obtained with Algorithm 2 are used to indicate the path indices where the systematic errors are likely to be present. Then, using this information, systematic errors, as large as 6%, as considered in case 3 of the numerical study, and

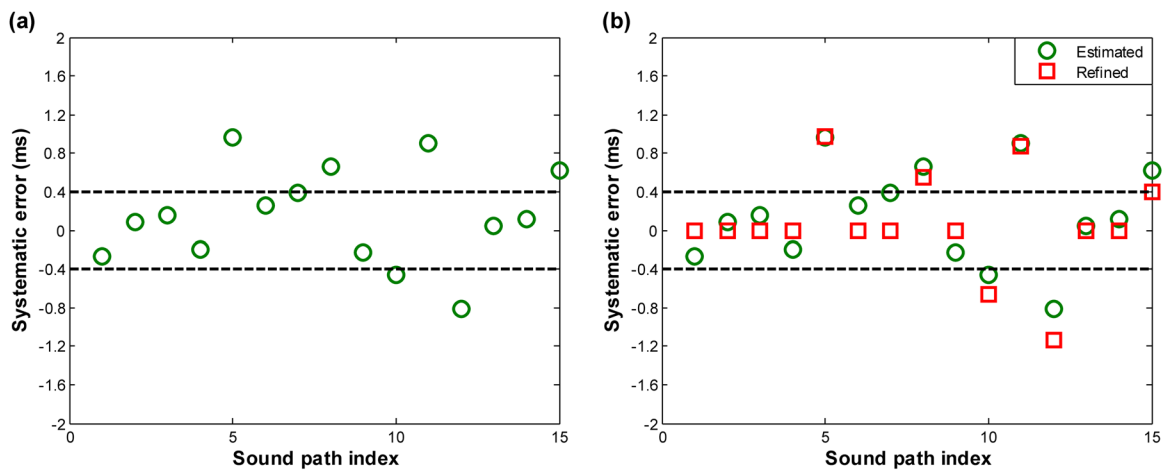

FIG. 8. (Color online) Systematic error analysis for the BAO experiment on 9 July 2008, 21:32 UTC. (a) Systematic errors estimated by Algorithm 2, assuming systematic errors in all paths. (b) Systematic errors estimated by the refined Algorithm 3, assuming systematic errors in paths 5, 8, 10, 11, 12, and 15.

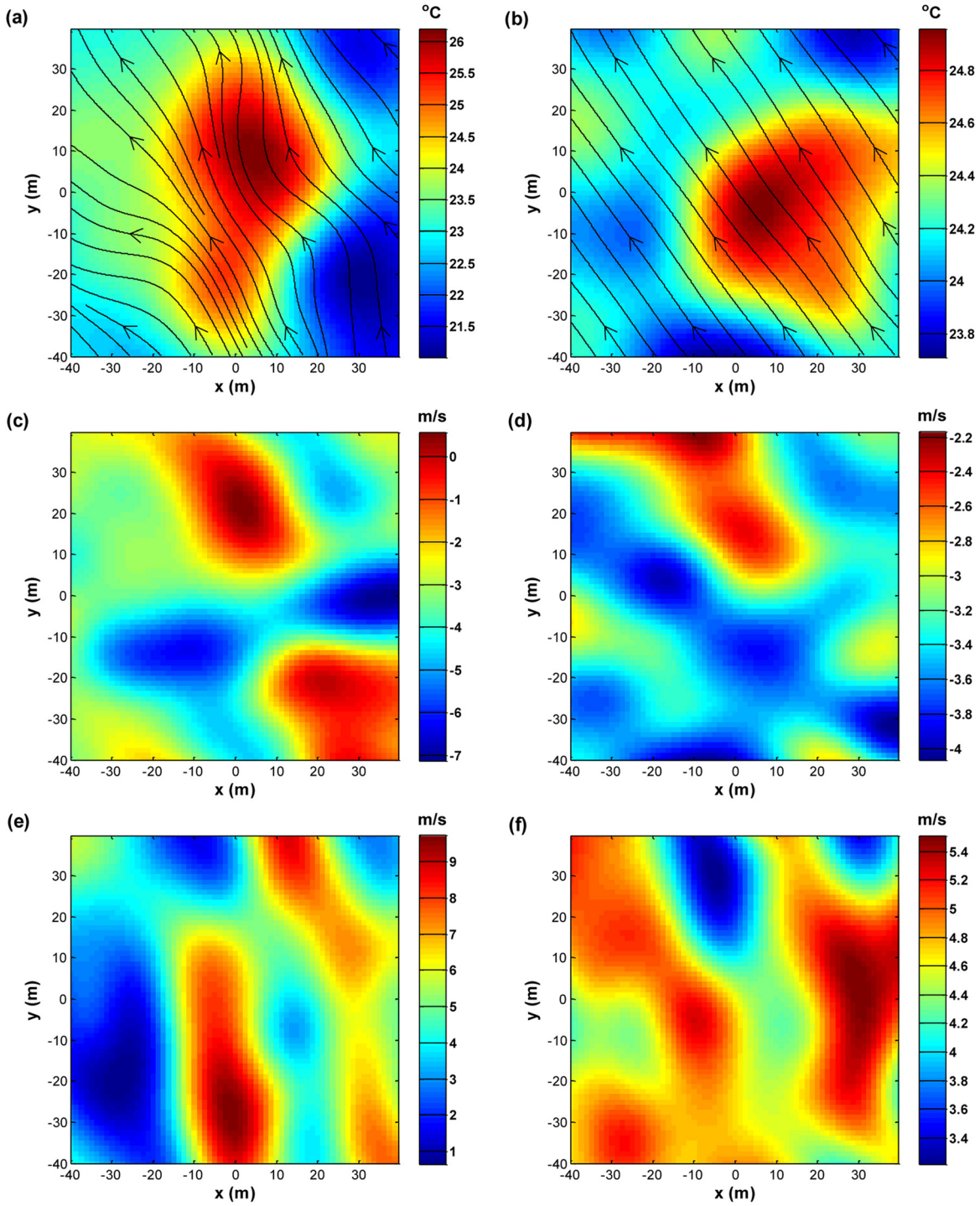

FIG. 9. (Color online) Reconstruction the fields in the BAO experiment on 11 August 2008, 21:31 UTC. Note significant improvement in reconstructions (right column) when Algorithm 3 was used. (a) Temperature field, no estimation of the systematic errors. (b) Temperature field, refined estimation of the systematic errors. (c) First horizontal component of the wind velocity vector, $u_0 + u$, no estimation of the systematic errors. (d) First horizontal component of the wind velocity vector, $u_0 + u$, refined estimation of the systematic errors. (e) Second horizontal component of the wind velocity vector, $v_0 + v$, no estimation of the systematic errors. (f) Second horizontal component of the wind velocity vector, $v_0 + v$, refined estimation of the systematic errors.

mean fields can be estimated more accurately by setting the remaining errors to zero (Algorithm 3).

The developed algorithms were studied numerically on several LES data sets corresponding to very unstable, unstable, and neutral atmosphere, and then applied to experimental data acquired at different conditions (day and night), although typical results and observed trends pertinent to two numerical and outdoor data sets were reported in the paper. The results obtained showed that expected errors decrease remarkably in the numerical and outdoor experiments and the reconstructions became more plausible, in the meaningful physical ranges for a given stability regime in the atmosphere.

As the suggested algorithms for assessment and elimination of systematic errors are general, they can be applied for other outdoor[31] and indoor[32] acoustic tomography arrays. However, particular results of this approach might depend

on the geometry of the transducers' locations in a tomography array. Therefore, further studies are necessary to assess effects for different arrays, their geometry and sizes, and fraction of the error-free measurements for successful application of the considered algorithms.

ACKNOWLEDGMENTS

This material is based upon work supported in part by the U.S. Army Research Laboratory and the U.S. Army Research Office under contract/grant number W911NF1010415. Permission to publish was granted by Director, Cold Regions Research and Engineering Laboratory.

[1]D. K. Wilson and D. W. Thomson, "Acoustic tomographic monitoring of the atmospheric surface layer," J. Atmos. Ocean. Technol. **11**, 751–769 (1994).
[2]A. Ziemann, K. Arnold, and A. Raabe, "Acoustic tomography in the atmospheric surface layer," Ann. Geophys. **17**, 139–148 (1999).
[3]P. Holstein, A. Raabe, R. Müller, M. Barth, D. Mackenzie, and E. Starke, "Acoustic tomography on the basis of travel-time measurement," Meas. Sci. Technol. **15**, 1420–1428 (2004).
[4]S. N. Vecherin, V. E. Ostashev, G. H. Goedecke, D. K. Wilson, and A. G. Voronovich, "Time-dependent stochastic inversion in acoustic travel-time tomography of the atmosphere," J. Acoust. Soc. Am. **119**(5), 2579–2588 (2006).
[5]S. N. Vecherin, V. E. Ostashev, A. Ziemann, D. K. Wilson, K. Arnold, and M. Barth, "Tomographic reconstruction of atmospheric turbulence with the use of time-dependent stochastic inversion," J. Acoust. Soc. Am. **122**(3), 1416–1425 (2007).
[6]S. N. Vecherin, V. E. Ostashev, D. K. Wilson, and A. Ziemann, "Time-dependent stochastic inversion in acoustic tomography of the atmosphere with reciprocal sound transmission," Meas. Sci. Technol. **19**(12), 125501 (2008).
[7]S. N. Vecherin, V. E. Ostashev, and D. K. Wilson, "Three-dimensional acoustic travel-time tomography of the atmosphere," Acta Acust. Acust. **94**(3), 349–358 (2008).
[8]J. L. Spiesberger, "Locating animals from their sounds and tomography of the atmosphere: Experimental demonstration," J. Acoust. Soc. Am. **106**(2), 837–846 (1999).
[9]S. A. Johnson, J. F. Greenleaf, C. R. Hansen, W. F. Samayoa, A. L. M. Tanaka, D. A. Christensen, and R. L. Wooley, "Reconstructing three-dimensional fluid velocity vector fields from acoustic transmission measurements," in *Acoustical Holography*, edited by L. W. Kessler, (Plenum, Berlin, 1977), Vol. 7, pp. 307–326.
[10]H. Braun and A. Hauck, "Tomographic reconstruction of vector fields," IEEE Trans. Signal Proc. **39**, 464–471 (1991).
[11]S. J. Norton, "Unique tomographic reconstruction of vector fields using boundary data," IEEE Trans. Image Proc. **1**, 406–412 (1992).
[12]I. Jovanović, L. Sbaiz, and M. Vetterli, "Acoustic tomography for scalar and vector fields: Theory and application to temperature and wind estimation," J. Atmos. Ocean Technol. **26**, 1475–1492 (2009).
[13]J. L. Spiesberger, "Ocean acoustic tomography: Travel time biases," J. Acoust. Soc. Am. **77**(1), 83–100 (1985).
[14]S. Kizu, "Systematic errors in estimation of insolation by empirical formulas," J. Oceanogr. **54**, 165–177 (1998).
[15]M. J. Martin, M. J. Bell, and N. K. Nichols, "Estimation of systematic error in an equatorial ocean model using data assimilation," Int. J. Num. Meth. Fluids **40**, 435–444 (2002).
[16]J. P. Hacker and D. L. Rife, "A practical approach to sequential estimation of systematic error on near-surface mesoscale grids," Weather Forecasting **22**(6), 1257–1273 (2007).
[17]R. G. Liu, J. Y. Liu, and S. Liang, "Estimation of systematic errors of MODIS thermal infrared bands," IEEE Geosci. Remote Sensing Lett. **3**(4), 541–545 (2006).
[18]Y. Yang, M. K. Cheng, C. K. Shum, and B. D. Tapley, "Robust estimation of systematic errors of satellite laser range," J. Geod. **73**(7), 345–349 (1999).
[19]J. L. Spiesberger and K. M. Fristrup, "Passive localization of calling animals and sensing of their acoustic environment using acoustic tomography," Am. Natural. **135**, 107–153 (1990).
[20]J. C. Santamarina and A. C. Reed, "Ray tomography: Errors and error functions," J. Appl. Geophys. **32**, 347–355 (1994).
[21]K. Arnold, A. Ziemann, and A. Raabe, "Tomographic monitoring of wind and temperature at different heights above the ground," Acta Acust. Acust. **87**, 703–708 (2001).
[22]P. P. Sullivan, J. C. McWilliams, and C.-H. Moeng, "A subgrid-scale model for large-eddy simulation of planetary boundary-layer flows," Boundary Layer Meteorol. **71**, 247–276 (1994).
[23]V. E. Ostashev, A. J. Bedard, S. N. Vecherin, D. K. Wilson, J. Leach, B. Bartram, C. Fairall, D. Wolfe, J. Jordan, R. Nishiyama, and K. A. Clark, "Acoustic tomography of the atmospheric surface layer at the Boulder Atmospheric Observatory," InterNoise Proc. **218**, 542–548 (2009).
[24]V. E. Ostashev, *Acoustics in Moving Inhomogeneous Media* (E & FN SPON, London, UK, 1997), 259 pp.
[25]K. Aki and P. G. Richards, *Quantitative Seismology*, 2nd ed. (University Science Books, Sausalito, CA, 2002), 704 pp.
[26]W. Munk, P. Worcester, and C. Wunsch, *Ocean Acoustic Tomography* (Cambridge Univ. Press, Cambridge, 1995), 433 pp.
[27]B. Cornuelle, "Simulations of acoustic tomography array performance with untracked or drifting sources and receivers," J. Geophys. Res. **90**(C5), 9079–9088, doi:10.1029/JC090iC05p09079 (1985).
[28]A. A. Silivra, J. L. Spiesberger, A. L. Fabrikant, and H. E. Hurlburt, "Acoustic tomography at basin scales and clock errors," IEEE J. Ocean Engin. **22**(1), 143–150 (1997).
[29]J. Hinze, *Turbulence* (McGraw-Hill, New York,1975).
[30]V. I. Tatarskii, *The Effects of the Turbulent Atmosphere on Wave Propagation* (Keter, Jerusalem, 1971).
[31]A. Raabe, K. Arnold, A. Ziemann, M. Schröter, S. Raasch, J. Bange, P. Zittel, Th. Spieb, Th. Foken, M. Göckede, F. Beyrich, and J.-P. Leps, "STINHO-STructure of turbulent transport under INHOmogeneous surface conditions—A micro-α scale field experiment and LES modelling," Meteorol. Z. **14**, 315–327 (2005).
[32]M. Seliger, M. Barth, and A. Raabe, "Akustische Lauzeittomographie in Ilmenauer Fass," Technical Report (Leipzig Insitute of Meteorology, Leipzig, Germany, 2005).